optica

Dissipative cnoidal waves (Turing rolls) and the soliton limit in microring resonators: supplementary material

ZHEN QI[1,*], SHAOKANG WANG[1], JOSÉ JARAMILLO-VILLEGAS[2], MINGHAO QI[3], ANDREW M. WEINER[3], GIUSEPPE D'AGUANNO[1], THOMAS F. CARRUTHERS[1], AND CURTIS R. MENYUK[1]

[1] University of Maryland at Baltimore County, 1000 Hilltop Circle, Baltimore, MD 21250, USA
[2] Technological University of Pereira, Cra. 27 10-02, Pereira, Risaralda 660003, Colombia
[3] Purdue University, 610 Purdue Mall, West Lafayette, IN 47907, USA
*Corresponding author: zhenqi1@umbc.edu

This document provides supplementary information for the article "Dissipative cnoidal waves (Turing rolls) and the soliton limit in microring resonators," https://doi.org/10.1364/OPTICA.6.001220. In Sec. S1, we show stability maps with normalized detuning. In Sec. S2, we discuss some features of the dynamical spectrum of the linearized Lugiato-Lefever equation. In Sec. S3, we give our formulation of the quantum noise modeling. In Sec. S4, we give a complete stability for the cnoidal waves where $L = 50$ and $-2 < \alpha < 6$. In Sec. S5, we derive an expression for the asymptotic behavior L/N_{per} as $L \to \infty$.

S1. STABILITY MAPS WITH NORMALIZED DETUNING

In this section, we show maps of the regions where stable wave solutions exist using the normalizations in Eq. (4). These plots are analogous to the plots in Figs. 3 and 8. In Fig. S1, we use the evolutionary method to find stationary solutions, and we integrate up to $t = 1000$. Each symbol in the figure corresponds to a different choice of the initial parameters h and δ. We show results for $L_\delta = 50$ and $L_\delta = 100$ with two different initial conditions. For the low-amplitude initial condition, we use an initial amplitude of 10^{-5} at $x = 0$, and for the high-amplitude initial condition, we use an amplitude of 10^5 at $x = 0$. The cnoidal wave solutions occupy an approximately cone-shaped region in the h-δ parameter space. Which cnoidal wave solution appears depends on the initial condition, as well as the parameters. In particular, low-periodicity cnoidal waves are never found with the low-amplitude initial condition. The lowest periodicity that we observed with $L_\delta = 50$ is $N_{\mathrm{per}} = 7$, and the lowest periodicity that we observed with $L_\delta = 100$ is $N_{\mathrm{per}} = 15$. By contrast, low-periodicity cnoidal waves, including solitons, can be obtained by starting with the high-amplitude initial condition. As

was the case with the normalization of Eq. (3), the location of the stability boundaries is ambiguous.

In Fig. S2, we show a map of the stable regions for $L_\delta = 50$ and $L_\delta = 100$ that we obtained using the dynamical approach. The self-similarity that we previously described in Sec. III is apparent. The stable regions for $N_{\mathrm{per}} = X$ at $L_\delta = 50$ are approximately the same as the stable regions for $N_{\mathrm{per}} = 2X$ at $L_\delta = 100$. As the periodicity increases, the loss that is necessary to obtain stable cnoidal waves also inreases. Hence, these stable solutions are disconnected from the lossless analytical solutions that we previously obtained [S1], which limits the utility of the analytical solutions.

S2. DYNAMICAL SPECTRUM OF THE LINEARIZED LLE

In this section, we will derive some properties of the dynamical spectrum of the linearized LLE.

It is useful to first transform $\Delta \boldsymbol{\Psi}$, given in Eqs. (6)–(8) to
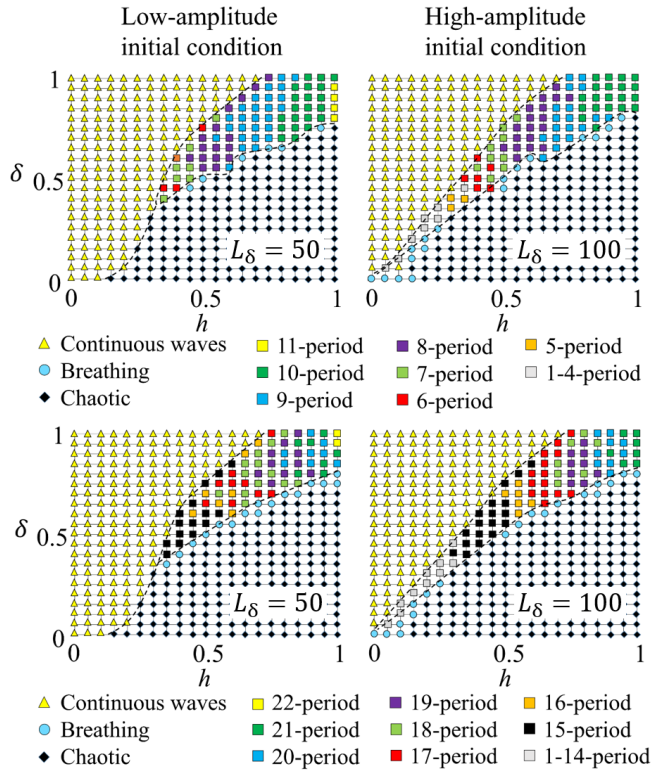
Fig. S1. We show a map of the solutions that emerge using the evolutionary approach for $L_\delta = 50$ and 100 and for two different initial conditions.

Fig. S2. Maps of the stable regions for cnoidal waves for $L_\delta = 10$, 25, 50 and 100.

remove the attenuation by defining

$$\Delta \mathbf{X} = \begin{bmatrix} \Delta\chi \\ \Delta\bar\chi \end{bmatrix} = \Delta\boldsymbol{\Psi}\exp t = \begin{bmatrix} \Delta\psi\exp t \\ \Delta\bar\psi\exp t \end{bmatrix}. \tag{S.1}$$

This transformation shifts all the eigenvalues by $+1$ so that the fourfold symmetry now appears with respect to the real and imaginary axes. We note that we have made no change in ψ_0, which has embedded in it the effects of both the pump and attenuation. We next let $\psi_0 = r_0 + is_0$, $\Delta\chi = r + is$, and $\Delta\bar\chi = r - is$. We also let $\mathbf{z}(t) = [r(t), s(t)]^T$, where we use T to denote the transpose so that $\mathbf{z}$ is a column vector. We now find
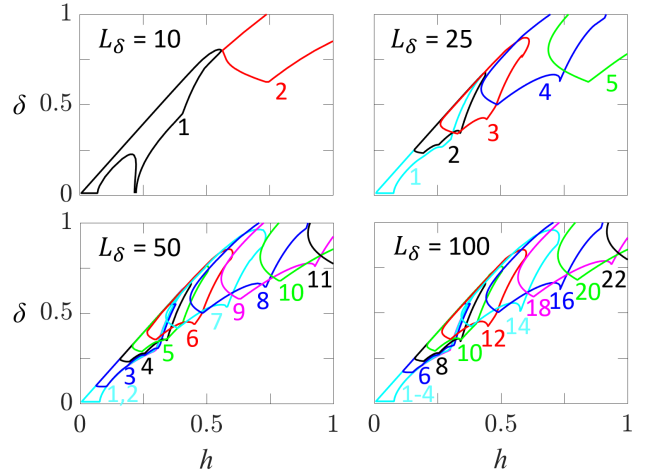
$$\frac{\partial \mathbf{z}}{\partial t} = \frac{\partial}{\partial t}\begin{bmatrix} r \\ s \end{bmatrix} = \begin{bmatrix} \mathbf{M}_{11} & \mathbf{M}_{12} \\ \mathbf{M}_{21} & \mathbf{M}_{22} \end{bmatrix} = \mathbf{M}\mathbf{z}, \tag{S.2}$$

where

$$\mathbf{M}_{11} = -2r_0 s_0, \qquad \mathbf{M}_{12} = -\frac{\partial^2}{\partial x^2} - r_0^2 - 3s_0^2 + \alpha,$$
$$\mathbf{M}_{21} = \frac{\partial^2}{\partial x^2} + 3r_0^2 + s_0^2 - \alpha, \qquad \mathbf{M}_{22} = 2r_0 s_0. \tag{S.3}$$

The operator $\mathbf{M}$ is real, which is sufficient to imply that if λ is a non-real eigenvalue, then λ^* is also an eigenvalue. Hence, the eigenvalues are symmetric with respect to the real axis. This same requirement holds for the linearized equation that corresponds to any variant of the scalar nonlinear Schrödinger equation, not just the LLE [S2].

The key to understanding the symmetry with respect to the imaginary axis is that the evolution equations that govern $\mathbf{z}(t)$

are Hamiltonian. These equations are derivable from the Hamiltonian

$$\mathcal{H} = \int_{-L/2}^{L/2} dx \left[\frac{1}{2}\left(\frac{\partial r}{\partial x}\right)^2 + \frac{1}{2}\left(\frac{\partial s}{\partial x}\right)^2 - \left(r_0^2 + s_0^2 - \frac{\alpha}{2}\right)(r^2 + s^2) \right.$$
$$\left. - \frac{1}{2}(r_0^2 - s_0^2)(r^2 - s^2) - 2r_0 s_0 rs \right]. \tag{S.4}$$

We then find $\partial r/\partial t = \mathrm{D}\mathcal{H}/\mathrm{D}s$ and $\partial s/\partial t = -\mathrm{D}\mathcal{H}/\mathrm{D}r$, where we use D to denote the functional derivative. Hence, we find that $r(x,t)$ is a canonical coordinate, parameterized by x, and that $s(x,t)$ is the corresponding canonical momentum. We may also write the evolution equations as

$$\frac{\partial \mathbf{z}}{\partial t} = \mathbf{M}z = \mathbf{J}\frac{\mathrm{D}\mathcal{H}}{\mathrm{D}\mathbf{z}}, \tag{S.5}$$

where $\mathbf{J}$ is the symplectic operator. It is defined by

$$\mathbf{J}\begin{bmatrix} a(x) \\ b(x) \end{bmatrix} = \begin{bmatrix} b(x) \\ -a(x) \end{bmatrix}, \tag{S.6}$$

where a and b are arbitrary functions of x. The operator $\mathbf{M}$ shares with all real Hamiltonian operators for linear systems the properties $\mathbf{M}_{22} = -\mathbf{M}_{11}^T$, $\mathbf{M}_{12} = \mathbf{M}_{12}^T$, and $\mathbf{M}_{21} = \mathbf{M}_{21}^T$ [S3]. We now find

$$\mathbf{J}(\mathbf{M} - \lambda \mathbf{I})\mathbf{J} = \mathbf{J}\mathbf{M}\mathbf{J} - \lambda\mathbf{J}^2 = \mathbf{M}^T + \lambda\mathbf{I}. \tag{S.7}$$

Since the eigenvalues of $\mathbf{M}$ and $\mathbf{M}^T$ are the same, we conclude that if λ is an eigenvalue, then so is $-\lambda$ and hence so is λ^*. So, the dynamical spectrum is symmetric about the imaginary axis.

We note parenthetically that this Hamiltonian formulation is a useful starting point for investigating quantum effects in microresonators.

We found that a number of the eigenvalues associated with the $N_\mathrm{per} = 8$ cnoidal waves are degenerate. Similar degeneracies occur with other cnoidal waves. Degeneracy is a consequence of translational symmetry. The length of one period of a cnoidal wave is L/N_per. It follows that if $\Delta\boldsymbol{\Psi}_{\lambda 1}(x)$ is an eigenvector with

an eigenvalue λ, then so is $\Delta\mathbf{\Psi}_{\lambda 1}(x + L/N_{\text{per}})$. We must be able to write

$$\Delta\mathbf{\Psi}_{\lambda 1}(x + L/N_{\text{per}}) = \sum_{m=1}^{M} c_m \Delta\mathbf{\Psi}_{\lambda m}(x), \qquad (S.8)$$

where the c_m are constants, the $\Delta\mathbf{\Psi}_{\lambda m}(x)$ are the eigenvectors that share the same eigenvalue λ, and M is the total number of eigenvectors that share that eigenvalue. If an eigenvalue is simple, then its eigenvector must have a period equal to L/N_{per}, which will not be the case in general. Thus, a high degree of degeneracy is expected for cnoidal waves with large N_{per}.

S3. QUANTUM NOISE SIMULATION

The fluctuating energy due to quantum noise is at least $h\nu$ per mode, where h is Planck's constant and ν is the central frequency of the mode. In a system with damping, nature must supply sufficient noise power to guarantee this noise level. The modes in a microresonator are spaced apart in frequency by the free spectral range (FSR) $1/T_R$, where T_R is the round-trip time. In practice, this fluctuating energy limit is just a lower limit. The actual fluctuating energy will typically be higher due to electromechanical and environmental noise sources [S4].

Writing $U_m = h\nu$ for the m-th mode, we obtain $P_m = h\nu/T_R$, where P_m is the corresponding power in the microresonator. It might seem strange that the noise power in mode m increases as the frequency separation increases. This increase occurs because the device size shrinks as the FSR increases, so that the energy density of each mode increases, and the amount of energy passing through any point of the microresonator per unit time increases.

The amplitude of the m-th mode is given by the Fourier transform of $A(\tau, \theta)$,

$$\tilde{A}_m(\tau) = \int_0^{2\pi} \frac{d\theta}{2\pi} A(\tau, \theta) \exp(-im\theta). \qquad (S.9)$$

The number of different modes that are kept in a simulation N_{mode} is equal to the number of node points in the simulation. We thus find that

$$\tilde{A}_m(\tau) = \frac{1}{N_{\text{mode}}} \sum_{j=1}^{N_{\text{mode}}} A(\tau, \theta_j) \exp(-im\theta_j) \qquad (S.10)$$

after discretization, where $\theta_j = 2\pi j/N_{\text{mode}}$. The average noise power due to quantum fluctuations is given by $P_m = \langle |\tilde{A}_{\text{noise},m}|^2 \rangle = h\nu/T_R$, where the brackets $\langle \cdot \rangle$ indicate an average over τ. We then find that the average noise power due to quantum fluctuations at each θ_j is given by $\langle |A_{\text{noise}}(\theta_j)|^2 \rangle = (h\nu/T_R)N_{\text{mode}}$. The loss due to attenuation must be compensated by vacuum fluctuations. In a system with just attenuation, we find [S5],

$$T_R \frac{d\tilde{A}_{\text{noise},m}}{d\tau} = -\frac{l}{2}\tilde{A}_{\text{noise},m} + R_m, \qquad (S.11)$$

where $\langle R_m(\tau)R_{m'}^*(\tau') \rangle = h\nu l \delta(\tau - \tau')\delta_{m,m'}$. It follows that the average change in $\tilde{A}_{\text{noise},m}$ in a small time step $\Delta\tau$ due to noise is given by

$$\langle |\Delta\tilde{A}_{\text{noise},m}|^2 \rangle = (h\nu/T_R)[1 - \exp(-l\Delta\tau/T_R)]$$
$$\simeq (h\nu/T_R)(l\Delta\tau/T_R). \qquad (S.12)$$

The corresponding change at each node point θ_j is given by $\langle |\Delta A(\theta_j)|^2 \rangle = (h\nu/T_R)(l\Delta\tau/T_R)N_{\text{mode}}$. The key point is that

vacuum fluctuations do not change in the presence of dispersion and an external pump that compensates for loss [S5]. Using the transformations following Eq. (1), we find that the corresponding changes in $\Delta\tilde{\psi}_m$ and $\Delta\psi(x_j)$ over a small time step Δt are given by $\langle |\Delta\tilde{\psi}_m|^2 \rangle = (2\gamma/l)(h\nu/T_R)2\Delta t$ and $\langle |\Delta\psi(x_j)|^2 \rangle = (2\gamma/l)(h\nu/T_R)2\Delta tN_{\text{mode}}$.

The computational algorithm is to add Gaussian-distributed random noise to the real and imaginary part of ψ at each node point θ_j, whose variance for each separately is equal to $(1/2)(2\gamma/l)(h\nu/T_R)2\Delta tN_{\text{mode}}$. Alternatively, one can add the noise in the wavenumber domain, using the variances for the real and imaginary parts of $\Delta\tilde{\psi}_m$.

For the parameters of Jaramallo-Villegas, et al. [S6] and assuming a step size that is $0.01T_R$, we first find that $l\Delta\tau/T_R = 2\Delta t = 0.02$. The noise power that must be added on each time is given by

$$\begin{aligned}
\langle |\Delta\tilde{A}_m|^2 \rangle &= (h\nu/T_R)(l\Delta\tau/T_R) \\
&= (6.63 \times 10^{-34})(2.0 \times 10^{14})(2.26 \times 10^{11})(0.02) \\
&= 5.99 \times 10^{-10}\,\text{W}.
\end{aligned}$$
$$(S.13)$$

If we assume that there are 512 nodes, which is a typical value in simulations, then we find that $\langle |\Delta A(\theta_j)|^2 \rangle = 3.07 \times 10^{-7}$ W. This power corresponds to approximately -35 dBm, which is small, but larger by about 200 dBm from the noise power due to roundoff noise in typical simulations. The corresponding value of $\langle |\Delta\tilde{\psi}_m|^2 \rangle$ is 6.03×10^{-18}, and the corresponding value of $\langle |\Delta\psi(x_j)|^2 \rangle$ is 3.09×10^{-15}.

S4. COMPLETE MAP OF THE STABLE REGIONS FOR $L = 50$

In Fig. S3, we show a map of the stable regions for all the cnoidal waves that are stable in the range $-2 < \alpha < 6$. This map is presented as a slide show in which one of the stable regions is highlighted in each slide.

S5. ASYMPTOTIC VALUE OF L/N_{per} AS $L \to \infty$

Here we calculate the most unstable wavenumber of continuous waves for parameters where cnoidal waves are stable and continuous waves are unstable. That allows us to predict analytically which cnoidal wave will form starting from noise when $L \to \infty$ and to obtain the asymptotic value of L/N_{per}. This procedure is similar to the one used by Godey et al. [S7] to predict which cnoidal wave will appear when continuous waves go unstable.

We start by assuming that ψ_0 is a complex constant. We then find that $\rho = |\psi_0|^2$ is given by the solution to the cubic equation

$$[1 + (\alpha - \rho)^2]\rho = F^2. \qquad (S.14)$$

We now perturb this solution, using the ansatz $\Delta\psi = \exp(\lambda t + ikx)$, $\Delta\bar{\psi} = \Delta\psi^*$. Substitution into Eq. (7) yields $\lambda = -1 \pm [\rho^2 - (2\rho - \alpha - k^2)^2]^{1/2}$. The growth rate λ is maximized when $dk/d\lambda = 0$, which implies $k = (2\rho - \alpha)^{1/2}$ or

$$L/N_{\text{per}} = 2\pi/k = \frac{2\pi}{(2\rho - \alpha)^{1/2}}. \qquad (S.15)$$

Substitution of the solution of Eq. (S.14) into Eq. (7) permits us to compute L/N_{per}. For $\alpha = -2$, $F = 3.5$, we find $L/N_{\text{per}} = 3.04$; for $\alpha = -1$, $F = 2.6$, we find $L/N_{\text{per}} = 3.43$; for $\alpha = 0$ and $F = 1.7$, we find $L/N_{\text{per}} = 4.07$; for $\alpha = 1$, $F = 1.2$, we find $L/N_{\text{per}} = 4.93$.

Fig. S3. A slide show map of all the stable regions for the cnoidal waves at $L = 50$ in the range $-2 < a < 6$. One of the stable regions is highlighted in each slide; the regions are labeled with their corresponding periodicity N_{per}. The red-dashed line shows the boundary below which continuous waves are stable.

REFERENCES

[S1] Z. Qi, G. D'Aguanno, and C. R. Menyuk, "Nonlinear frequency combs generated by cnoidal waves in microring resonators," J. Opt. Soc. Am. B **34**, 785–794 (2017).

[S2] C. R. Menyuk and S. Wang, "Spectral methods for determining the stability and noise performance of passively modelocked lasers," Nanophotonics **5**, 332–350 (2016).

[S3] K. R. Meyer, G. R. Hall, and D. Offin, *Introduction to Hamiltonian Systems and the N-Body Problem* [Second Edition] (Springer, 2009). See Sec. 3.3.

[S4] W. Liang, D. Eliyahu, V. S. Ilchenko, A. B. Matsko, D. Seidel, and L. Maleki, "High spectral purity Kerr frequency comb radio frequency photonic oscillator," Nat. Comm. **6**, 7957 (2015).

[S5] R. Loudon, *The Quantum Theory of Light* (Oxford, 1983). See Chap. 7.

[S6] J. A. Jaramillo-Villegas, X. Xue, P.-H. Wang, D. E. Leaird, and A. M. Weiner, "Deterministic single soliton generation and compression in microring resonators avoiding the chaotic region," Opt. Exp. **23**, 9618–9626 (2015).

[S7] C. Godey, I. V. Balakireva, A. Coillet, and Y. K. Chembo, "Stability analysis of the spatiotemporal Lugtiato-Lefever model for Kerr optical frequency combs in the anomalous and normal dispersion regimes," Phys. Rev. A **89**, 063814 (2014).